ACS Photonics

Letter

pubs.acs.org/journal/apchd5

Microwave Funneling through Sub-10 nm Nanogaps

Kwanghee Lee,[†] Jeeyoon Jeong,[†] Young-Mi Bahk,[†] Jiyeah Rhie,[†] In-Keun Baek,[‡] Bong Jun Lee,[†] Yu Hyun Kang,[†] Seunghun Hong,[§] Gun-Sik Park,[‡] and Dai-Sik Kim*[,†]

[†]Department of Physics and Astronomy and Center for Atom Scale Electromagnetism, [‡]Center for THz-Bio Application Systems, Department of Physics and Astronomy, and [§]Department of Physics and Astronomy, Department of Biophysics and Chemical Biology, and Institute of Applied Physics, Seoul National University, Seoul 08826, Republic of Korea

ABSTRACT: We demonstrate microwave funneling through metallic gaps of nanometer-scale width, corresponding to $\lambda/10\,000\,000$. For achieving both resonant transmission and strong confinement of microwaves, we fabricate two types of samples with an extreme aspect ratio: 300 nm wide, 3.5 mm long slots and sub-10 nm wide rectangular rings with a perimeter of 6.5 mm. Considering the peak transmittance value of 45% and the small coverage ratio of transparent area in the nanogap surface, we can infer a giant intensity enhancement factor of up to 25 million inside the nanogaps. The polarization extinction ratio up to 20 dB indicates that the microwave transmission originates from capacitive coupling of the induced charges at the sidewalls of a metallic gap. We also measure terahertz transmittance and observe a convergence to the microwave range. Our work represents the highest field enhancement recorded for the microwave regime, made possible by wafer-scale-length nanogaps matching the wavelengths, with future applications in centimeter wave nonlinearities and enhanced detection sensitivities.

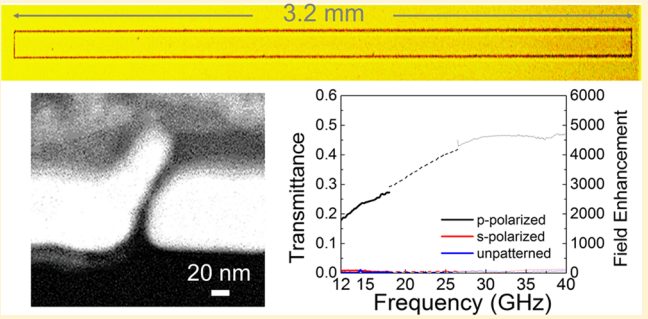

KEYWORDS: *light confinement, microwave, terahertz spectroscopy, nanogap, atomic layer lithography*

Electromagnetic wave confinement into subwavelength metallic structures has been intensely studied in a broad range of geometries and frequencies.[1−6] Recently, light confinement has been achieved at a few-nanometer-wide apertures[7−9] and even at an angstrom scale.[10,11] Such strong confinement of electromagnetic wave enables not only improved applications, e.g., surface-enhanced Raman scattering sensors,[12,13] molecule detectors for small quantities,[14] and insulator-to-metal phase transition metamaterials,[15,16] but also novel observations of boosted multiphoton processes,[17,18] nonlocal effects,[19] Fowler−Nordheim tunneling,[20] terahertz quantum plasmonics at the supernanometer regime,[21] etc. In principle, the squeezing of electromagnetic waves onto subwavelength metallic structures can be achieved at arbitrary frequency and length scales. However, at longer wavelength regimes, i.e., microwave and radio frequencies, the degree of wave confinement has been limited to micrometer-scale apertures.[22−25] Although there have been microwave studies concerned with the nanoscale such as nanomaterial characterization,[26] near-field probing,[27] and superconducting circuitry,[28] these works are not in the context of electromagnetic wave confinement. The main reason that hinders further studies of microwave confinement is a lack of a fabrication method satisfying both nanometer-scale feature size and millimeter-scale pattern size. Even though electron-beam or focused-ion-beam lithography can be utilized to fabricate few-millimeter-long nanostructures, such serial writing techniques are time-consuming and cost-ineffective.

In this paper, we demonstrate extreme squeezing of microwaves into nanometer-wide metallic structures to push the limit of the light confinement at the nanoscale toward the lowest frequency regime. We prepare two types of samples with an extreme aspect ratio: 300 nm wide, 3.5 mm long nanoslots and sub-10 nm wide rectangular nanogap rings with a perimeter of 6.5 mm, made by focused ion beam (FIB) and atomic layer lithography,[8,9,29] respectively. Atomic layer lithography, a recently developed nanofabrication process, predefines the pattern of metallic structures by photolithography and forms a dielectric spacer using atomic layer deposition. This method is free from the trade-off between resolution and pattern size, found in most top-down lithography techniques, thus enabling atomic-scale resolution of width while maintaining enough length for a resonant microwave transmission. To confirm the funneling of an electromagnetic wave through the nanogap structures, we measure microwave transmission by open-ended waveguide pairs connected with a vector network analyzer (VNA) and also perform terahertz time-domain spectroscopy (THz-TDS). We observe strong transmittance of 30% from the 300 nm wide nanoslots and 50% from the sub-10 nm wide nanogap rings at a wavelength of 1 cm. A microwave can funnel through the gaps with a size corresponding to ten millionth of its wavelength, Considering the gaps cover only 0.023% and 0.01% of the sample surfaces, the magnitudes of electric fields

Received: January 21, 2016
Published: March 16, 2016

DOI: 10.1021/acsphotonics.6b00047
ACS Photonics 2016, 3, 537−542

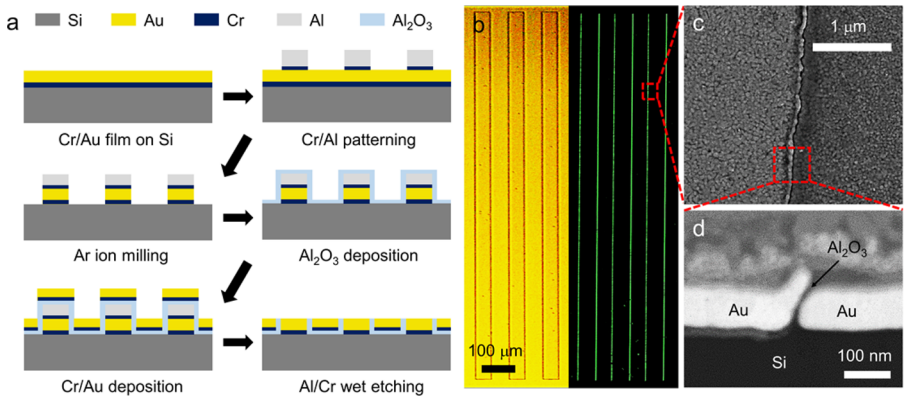

Figure 1. Nanogaps for resonant microwave transmission. (a) Atomic layer lithography process consisting of metal deposition, photolithography, ion milling, atomic layer deposition, and chemical etching. (b) Top-view optical micrographs of a 50 μm × 3200 μm rectangular ring array with a sub-10 nm wide gap. The images are reduced in the vertical direction to show the whole ring structure. (Left) Reflection image (right) dark field image under p-polarized illumination. (c) Top-view SEM image. (d) Cross sectional SEM image.

inside the gaps increase up to *1400-fold* and *5000-fold*, for the *nanoslots* and the *nanogap rings*, respectively.[30,31] The essential physics is as follows: incident magnetic-field-induced current density of $2H_{inc}/h$ (h = film thickness) charges the gap, which translates into huge electric field enhancement on the order of $\frac{\lambda}{\pi n h}$ where n is the index of refraction.[32,33]

The nanogap samples used in this work are made by two different techniques. The 300 nm wide nanoslots are milled by FIB, after deposition of 3 nm thick chromium as an adhesion layer and 97 nm thick gold on an undoped silicon substrate. The sub-10 nm wide nanogap rings are fabricated by modified atomic layer lithography with chemical etching to ensure high-throughput fabrication[29] since the microwave beam size is much larger than that of optics and millimeter waves. Figure 1a shows the fabrication process of the nanogap rings. We first deposit chromium and gold on the silicon substrate and make aluminum mask patterns with an adhesion layer by standard photolithography. The patterned sample is milled by Ar ions to form the outer region of the nanogap rings, and the alumina (Al_2O_3) spacer layer is coated by atomic layer deposition. After the coating, chromium and gold are deposited again to fill the rings, and the gap is revealed by removing the aluminum mask via chemical etching. Unlike the taping method used to peel off the excess metal,[8] chemical etching can be performed under well-defined and uniform conditions and thus provides high-throughput fabrication. Moreover, the fabricated nanogaps are highly rigid since both metallic regions surrounding the spacer are deposited with the adhesion layer. We can confirm the long and uniform dielectric gap formation by the optical reflection and dark field top-view images (Figure 1b) and the scanning electron microscope (SEM) top-view image (Figure 1c) of the nanogap rings. The SEM cross section of the nanogap ring (Figure 1d) clearly shows a dielectric gap of sub-10 nm width.

We measure microwave transmittances of the nanogap samples to observe funneling behavior. The sample is sandwiched by open-ended waveguide pairs connected with a VNA (Figure 2b). Three open-ended waveguide pairs are used to cover a 12−40 GHz range with the fundamental TE_{10} mode. Each open-ended waveguide pair is calibrated by a thru-reflect-line standard before measurement. Figure 3 is the microwave transmittances of both nanogap samples and the unpatterned gold film under p- and s-polarized incident waves. Transmitted microwave amplitudes from the samples are normalized with

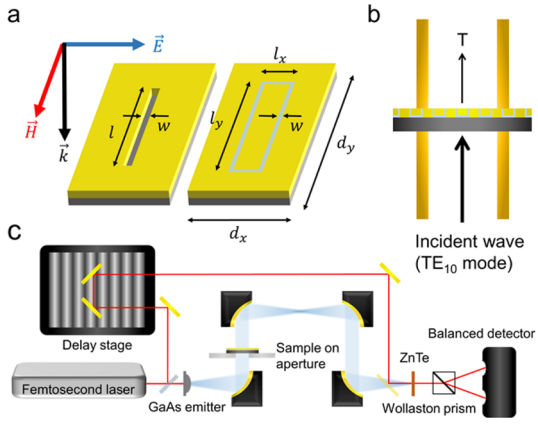

Figure 2. Illustrations of the samples and the experimental apparatus. (a) Schematic of the nanoslot and the nanogap ring with a p-polarized incident wave. (b) Cross section of the experimental setup for the microwave range. The samples are sandwiched between open-ended rectangular waveguide pairs connected with a vector network analyzer. (c) Experimental setup for THz-TDS measurement. The collimated THz beam illuminates the samples mounted on the metallic aperture.

those of bare substrates. The microwave transmittances under p-polarization show broad but resonant features and are clearly distinguished from that of s-polarization and unpatterned gold film. The polarization extinction ratio reaches up to 20 dB at the peak transmittance of the nanogap rings. This strong transmission of p-polarized waves indicates the capacitive coupling of induced charges and electric field enhancement at the gaps, as reported in previous studies in the THz range.[31] Although the skin depth of gold in the microwave regime (about 700 nm) is much larger than the thickness of the sample (97 nm), most of the incident wave is reflected at the metal−air interface due to the high permittivity of gold. Therefore, direct transmission through the metal layer is very low (~0.5%) and spectrally flat, resulting in the near-zero transmittance of the unpatterned gold film shown in Figure 3. Clearly, funneling at the nanogaps dominates the transmission.

We perform THz-TDS on the samples for comparison with microwave transmittance (Figure 2c). To avoid evanescent decay from a small aperture below a cutoff frequency and any effects from frequency-dependent spot sizes, the samples are mounted on large aluminum apertures (1 cm × 1 cm for the nanoslots, 1.6 cm × 1.6 cm for the nanogap rings) and

DOI: 10.1021/acsphotonics.6b00047
ACS Photonics 2016, 3, 537−542

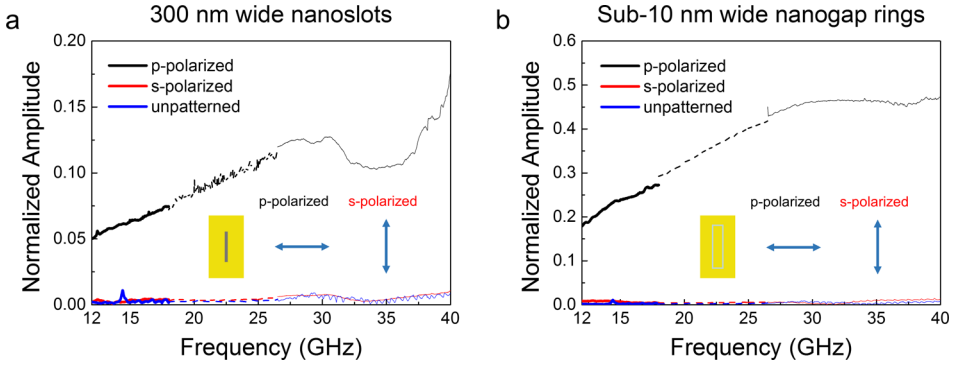

Figure 3. Microwave transmittances through the nanogaps. (a) Microwave transmittance of the 300 nm wide nanoslot antenna array. l = 3.5 mm, d_x = 1 mm, and d_y = 4.5 mm. (b) Microwave transmittance of the sub-10 nm wide nanogap rings array. l_x = 50 μm, l_y = 3200 μm, d_x = 100 μm, and d_y = 3250 μm. Transmitted amplitudes of the samples with p- and s-polarized incident waves and unpatterned gold film of the same thickness are normalized with those of the bare substrate. Transmittances are measured in the three frequency ranges K_u (12−18 GHz, thick solid), K (18−26.5 GHz, dashed), and K_a (26.5−40 GHz, thin solid) band.

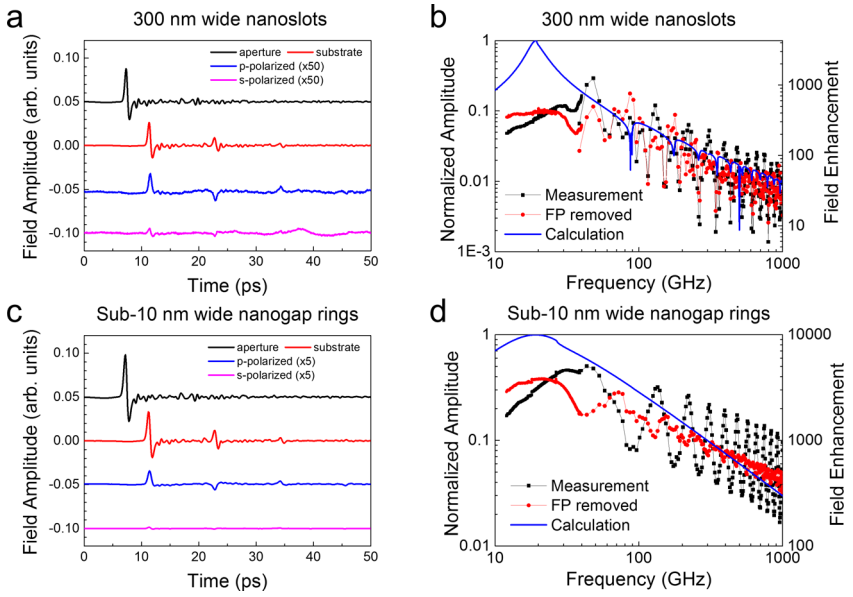

Figure 4. THz transmittances through the nanogaps. (a) Time traces of transmitted THz wave through the 300 nm wide nanoslots. (b) Microwave and THz transmittance of the nanoslots. (c) Time traces of transmitted THz wave through the sub-10 nm wide nanogap rings. (d) Microwave and THz transmittance of the nanogap rings. THz transmittances are obtained by a THz-TDS setup of 5 GHz frequency resolution, the reciprocal of the 200 ps scanning time range.

illuminated by a collimated THz beam. The scanning time is set at 200 ps for capturing low-frequency components. The frequency resolution is 5 GHz, the reciprocal of the scanning time. Figure 4a and c are time traces of a transmitted THz wave through a bare aluminum aperture, substrate, and the nanogaps under p- and s-polarizations. Multiple peaks with 11.45 ps intervals from the substrate originate from the Fabry−Pérot (FP) resonance related to a thickness of 500 μm and a refractive index of 3.435, nearly a constant value in the frequency range of interest.[34,35] The sign of the second peak from the nanogaps is inverted due to π-phase shift at the metal−substrate interface. Figure 4b and d are the log-scale plots of microwave and THz transmittance of the nanoslots and the nanogap rings, respectively. We subtract the transmitted THz amplitude through an unpatterned gold film in the time domain, calculate the transmitted amplitude spectra by Fourier transform, and finally obtain transmittance by normalization with the bare substrate. Microwave and THz transmittance measurements are fully consistent within their respective overlap regions, enabling a unified picture of the whole range. A slight mismatch of transmittance in Figure 4b is mainly due to a low signal-to-noise ratio of THz-TDS at the lower limit of frequency and does not break the consistency of the experiments. We deduce the electric field enhancement factor of the nanogaps by dividing the normalized transmitted amplitude by the coverage ratio of the gap area in the sample surface.[31] The peak values of the field enhancement reach 1400 for the 300 nm wide nanoslots and 5000 for the nanogap rings with a 5 nm gap width (estimated by Figure 1d). These giant values are still below the theoretical limit of the slit structure[36] and the experimental record of the nanogap rings in the THz regime,[8] due to the overpopulation of patterns in the samples.[37] We expect to achieve further enhancement of the microwave field inside the nanogaps with optimized geometries.

The fundamental resonance of the ring structure occurs when the perimeter of the ring matches the wavelength, after having taken care of the effective index of refraction of the air−substrate composite.[38] On the other hand, the fundamental

DOI: 10.1021/acsphotonics.6b00047
ACS Photonics 2016, 3, 537−542

resonance of the slot structure takes place when the length of the slot matches a half of wavelength. In this work, the length of the nanoslot is 3.5 mm and the perimeter of the nanogap ring is 6.5 mm. Owing to these length scales and substrate effect, theoretically expected resonance frequencies of both samples fall into the centimeter wave range. Calculations by the modal expansion method[30] with consideration of the gap plasmon[39] (blue lines in Figure 4b and d) predict the fundamental resonances of both samples at 19 GHz, departing significantly from the experimental peaks occurring at wavelength of about 1 cm (30−40 GHz) for both samples. The effects of FP resonances on the measured transmittances can be partially removed by straightforward calculations from air−substrate−air problems[40] (red lines in Figure 4b and d), with consideration of the π-phase shift from the metal−substrate interface, and the results show fundamental resonance peaks agreeing better with calculations.

It is noted that experiments and calculations agree well at terahertz frequency ranges, while the experimental enhancement values are significantly smaller at microwave frequencies. The differences of experimental and theoretical transmittance magnitudes may come from nonzero conductivity of the substrate, density of patterns, fabrication errors, etc. For the nanoslots case, the fabrication process is straightforward, and thus the conductivity of the substrate and the sparsity of the slots would be dominant. On the other hand, the transmittance of the nanogap rings can be significantly affected by imperfections of the samples such as asymmetric periodicity,[41] tapered gap opening,[42] defects of dielectric spacer, and debris from the chemically etched metal. In particular, the defects of the spacer and the metallic debris can be treated as small metallic bridges in or on the gaps. These metallic bridges provide an interesting perspective on the particle sensing with microwaves. At the high-frequency regime, the nanoslots and the nanogap rings would behave as infinite slit structures due to their length and perimeter of over 3 mm.[31] The metallic bridges would change the high-frequency transmittances of the slits from nonresonant to high-order resonant responses, and the difference of these two responses is small in terms of the peak magnitude.[43] On the other hand, the fundamental resonances of the nanoslots and the nanogap rings would be dominant at the low-frequency regime, and these are intimately affected by the small bridges of individual slots or rings.[44,45] Therefore, surprisingly, microwaves may be more sensitive than THz and visible light to the overall defects of the whole ring structure, making it a useful tool to investigate wafer-scale uniformity.

In conclusion, we demonstrate microwave funneling through 300 nm wide nanoslots and sub-10 nm wide nanogap rings. The nanoslots are milled by FIB, and the nanogap rings are fabricated by atomic layer lithography. Microwave and THz transmittances reach up to 30% for the nanoslots and 50% for the nanogap rings. By considering the 0.01% coverage ratio of the gap area in the sample surface, estimated field enhancement factors reach values of 1400 and 5000. The fundamental resonances are at wavelengths of about 1 cm, due to the combination of the nanogap geometries and FP resonances from the substrates. This work is the first demonstration of resonant microwave transmission through nanometer-sized structures, squeezing an electromagnetic wave in the $\lambda/10\,000\,000$ scale. Our work paves the way to the extreme confinement of microwaves into the nanoscale, applicable to low-frequency applications of enhanced nonlinearities and detection sensitivity.

METHODS

Nanogap Fabrication. We make the nanoslots by stitching of FIB (FIB200, FEI) milling of a 100 nm thick metal film (3 nm chromium and 97 nm gold) thermally evaporated on undoped silicon substrate (500 μm thick, 1000 Ω·cm). We also fabricate the nanogap rings by modified atomic layer lithography using chemical etching to expose the gaps, as reported in our previous work.[29] We first deposit 3 nm thick chromium as an adhesion layer and 97 nm thick gold on the undoped silicon substrate (500 μm thick, 1000 Ω·cm) by thermal evaporator. We pattern a 150 nm thick aluminum and 30 nm thick chromium sacrificial layer by standard photolithography (AZ5214E, image reversal). The patterned sample is milled by Ar ions (0.5 nm/min etching rate, 5 min for the top and 5 min for the sidewall) to form the outer region of the nanogap rings. The alumina (Al_2O_3) spacer layer is then coated by atomic layer deposition (1.1 Å/cycle at 250 °C). After coating the spacer, chromium and gold are deposited again to fill inside the rings, and the gaps are exposed by chemical etching of aluminum (KOH, 45%) and chromium (CR-7, Cyantek).

Sample Images. We use an optical reflection microscope and a field-enhanced scanning electron microscope (FE-SEM, TESCAN) to obtain top-view and cross sectional images of the samples. To gain an optical dark field image, we slant the nanogap rings so that reflected beams would not be collected by the objective lens (5×, numerical aperture (NA) = 0.15) and only scattered light from the nanogaps can be imaged. Asymmetric lines of the dark field image are due to the slanted angle of the sample. To acquire the cross sectional image, we deposit platinum on the gap and cut by focused ion beam combined with FE-SEM. Platinum on the top prevents damage to the nanogaps while proceeding with gallium ion beam milling.

Microwave Transmittance Measurement. We measure microwave transmittances by three open-ended rectangular waveguide pairs (62EWGN, 42EWGK, and 28EWGK, Chengdu AINFO Inc.) connected with the VNA (Vectorstar MS4644A, Anritsu). The aperture sizes of open-ended waveguides are WR62 (15.80 mm × 7.90 mm) for the K_u band (12−18 GHz), WR42 (10.67 mm × 4.32 mm) for the K band (18−26.5 GHz), and WR28 (7.11 mm × 3.56 mm) for the K_a band (26.5−40 GHz), supporting the fundamental TE_{10} mode for the corresponding frequency band. We polish waveguide apertures to be planar, smooth, and parallel to the sample surface. After aligning each waveguide pair, we perform thru-reflect-line calibration (241, 851, and 401 data points for K_u, K, and K_a bands, respectively) using homemade waveguide calibration kits. The lengths of "line" standards (90° phase shift of the center frequency of the band) are 6.31, 4.34, and 2.92 mm for the K_u, K, and K_a band, respectively. Power from the VNA is about 10 mW, far below the breakdown limit of the dielectric spacer and nonlinear regime.[21] We insert the samples in the center of the calibrated waveguide pairs and gently clamp by the waveguide pairs so they make contact with no air gap. Transmittances are reproducible, although we press the samples while measuring. We measure several times while slightly rotating the samples and select two angles with maximum and minimum transmittance as the p- and s-polarization cases.

THz-TDS. We perform THz-TDS to measure millimeter-wave transmittance from 40 to 1000 GHz. We divide a laser beam of 130 fs pulse width, 800 nm center wavelength, and 80

DOI: 10.1021/acsphotonics.6b00047
ACS Photonics 2016, 3, 537−542

MHz repetition rate (Mira 900 and Verdi V5, Coherent) into pump and probe beams. The pump beam impinges on a GaAs emitter to generate a THz beam. A collimated THz beam of 2 cm diameter illuminates the samples mounted on a 1.6 cm × 1.6 cm aluminum aperture. Estimated electric field strength at the sample is about 3 V/cm, not enough to observe any nonlinear phenomena.[11,21] The transmitted beam is collected by parabolic mirrors (NA = 0.32) and detected by electro-optic sampling with a (110)-oriented ZnTe crystal. The scanning time is set to 200 ps with a 0.05 ps resolution. Each transmittance is measured 30 times and averaged to enhance the signal-to-noise ratio.

AUTHOR INFORMATION

Corresponding Author

*E-mail: dsk@phya.snu.ac.kr.

Author Contributions

The manuscript was written through contributions of all authors. All authors have given approval to the final version of the manuscript.

Notes

The authors declare no competing financial interest.

ACKNOWLEDGMENTS

This work was supported by the National Research Foundation of Korea (NRF) grant funded by the Korean government (MSIP: NRF-2015R1A3A2031768, NRF-2009-0083512, and H-GUARD 2013M3A6B2078961) (MOE: BK21 Plus Program-21A20131111123). We thank Dr. Sun-Hong Min for valuable comments and Jaiu Lee for helpful assistance.

REFERENCES

(1) Ebbesen, T. W.; Lezec, H. J.; Ghaemi, H. F.; Thio, T.; Wolff, P. A. Extraordinary optical transmission through sub-wavelength hole arrays. *Nature* **1998**, *391*, 667−669.

(2) Lee, J. W.; Seo, M. A.; Kim, D. S.; Jeoung, S. C.; Lienau, C.; Kang, J. H.; Park, Q.-H. Fabry−Perot effects in THz time-domain spectroscopy of plasmonic band-gap structures. *Appl. Phys. Lett.* **2006**, *88*, 071114.

(3) Miyazaki, H. T.; Kurokawa, Y. Squeezing Visible Light Waves into a 3-nm-Thick and 55-nm-Long Plasmon Cavity. *Phys. Rev. Lett.* **2006**, *96*, 097401.

(4) Seo, M. A.; Adam, A. J. L.; Kang, J. H.; Lee, J. W.; Ahn, K. J.; Park, Q. H.; Planken, P. C. M.; Kim, D. S. Near field imaging of terahertz focusing onto rectangular apertures. *Opt. Express* **2008**, *16*, 20484−20489.

(5) Garcia-Vidal, F. J.; Martin-Moreno, L.; Ebbesen, T. W.; Kuipers, L. Light passing through subwavelength apertures. *Rev. Mod. Phys.* **2010**, *82*, 729−787.

(6) Nien, L.-W.; Lin, S.-C.; Chao, B.-K.; Chen, M.-J.; Li, J.-H.; Hsueh, C.-H. Giant Electric Field Enhancement and Localized Surface Plasmon Resonance by Optimizing Contour Bowtie Nanoantennas. *J. Phys. Chem. C* **2013**, *117*, 25004−25011.

(7) Ciraci, C.; Hill, R. T.; Mock, J. J.; Urzhumov, Y.; Fernandez-Dominguez, A. I.; Maier, S. A.; Pendry, J. B.; Chilkoti, A.; Smith, D. R. Probing the ultimate limits of plasmonic enhancement. *Science* **2012**, *337*, 1072−1074.

(8) Chen, X.; Park, H. R.; Pelton, M.; Piao, X.; Lindquist, N. C.; Im, H.; Kim, Y. J.; Ahn, J. S.; Ahn, K. J.; Park, N.; Kim, D. S.; Oh, S. H. Atomic layer lithography of wafer-scale nanogap arrays for extreme confinement of electromagnetic waves. *Nat. Commun.* **2013**, *4*, 2361.

(9) Chen, X.; Park, H. R.; Lindquist, N. C.; Shaver, J.; Pelton, M.; Oh, S. H. Squeezing millimeter waves through a single, nanometer-wide, centimeter-long slit. *Sci. Rep.* **2014**, *4*, 6722.

(10) Ward, D. R.; Huser, F.; Pauly, F.; Cuevas, J. C.; Natelson, D. Optical rectification and field enhancement in a plasmonic nanogap. *Nat. Nanotechnol.* **2010**, *5*, 732−736.

(11) Bahk, Y. M.; Kang, B. J.; Kim, Y. S.; Kim, J. Y.; Kim, W. T.; Kim, T. Y.; Kang, T.; Rhie, J.; Han, S.; Park, C. H.; Rotermund, F.; Kim, D. S. Electromagnetic Saturation of Angstrom-Sized Quantum Barriers at Terahertz Frequencies. *Phys. Rev. Lett.* **2015**, *115*, 125501.

(12) Siegfried, T.; Wang, L.; Ekinci, Y.; Martin, O. J. F.; Sigg, H. Metal double layers with sub-10 nm channels. *ACS Nano* **2014**, *8*, 3700−3706.

(13) Zhang, Q.; Large, N.; Nordlander, P.; Wang, H. Porous Au Nanoparticles with Tunable Plasmon Resonances and Intense Field Enhancements for Single-Particle SERS. *J. Phys. Chem. Lett.* **2014**, *5*, 370−374.

(14) Park, H. R.; Ahn, K. J.; Han, S.; Bahk, Y. M.; Park, N.; Kim, D. S. Colossal absorption of molecules inside single terahertz nanoantennas. *Nano Lett.* **2013**, *13*, 1782−1786.

(15) Liu, M.; Hwang, H. Y.; Tao, H.; Strikwerda, A. C.; Fan, K.; Keiser, G. R.; Sternbach, A. J.; West, K. G.; Kittiwatanakul, S.; Lu, J.; Wolf, S. A.; Omenetto, F. G.; Zhang, X.; Nelson, K. A.; Averitt, R. D. Terahertz-field-induced insulator-to-metal transition in vanadium dioxide metamaterial. *Nature* **2012**, *487*, 345−348.

(16) Jeong, Y. G.; Han, S.; Rhie, J.; Kyoung, J. S.; Choi, J. W.; Park, N.; Hong, S.; Kim, B. J.; Kim, H. T.; Kim, D. S. A Vanadium Dioxide Metamaterial Disengaged from Insulator-to-Metal Transition. *Nano Lett.* **2015**, *15*, 6318−6323.

(17) Lassiter, J. B.; Chen, X.; Liu, X.; Ciracì, C.; Hoang, T. B.; Larouche, S.; Oh, S.-H.; Mikkelsen, M. H.; Smith, D. R. Third-Harmonic Generation Enhancement by Film-Coupled Plasmonic Stripe Resonators. *ACS Photonics* **2014**, *1*, 1212−1217.

(18) Jensen, R. A.; Huang, I. C.; Chen, O.; Choy, J. T.; Bischof, T. S.; Lončar, M.; Bawendi, M. G. Optical Trapping and Two-Photon Excitation of Colloidal Quantum Dots Using Bowtie Apertures. *ACS Photonics* **2016**, *3*, 423.

(19) Mortensen, N. A.; Raza, S.; Wubs, M.; Søndergaard, T.; Bozhevolnyi, S. I. A generalized non-local optical response theory for plasmonic nanostructures. *Nat. Commun.* **2014**, *5*, 3809.

(20) Wu, L.; Duan, H.; Bai, P.; Bosman, M.; Yang, J. K. W.; Li, E. Fowler−Nordheim Tunneling Induced Charge Transfer Plasmons between Nearly Touching Nanoparticles. *ACS Nano* **2013**, *7*, 707−716.

(21) Kim, J. Y.; Kang, B. J.; Park, J.; Bahk, Y. M.; Kim, W. T.; Rhie, J.; Jeon, H.; Rotermund, F.; Kim, D. S. Terahertz Quantum Plasmonics of Nanoslot Antennas in Nonlinear Regime. *Nano Lett.* **2015**, *15*, 6683−6688.

(22) Yang, F.; Sambles, J. R. Resonant transmission of microwaves through a narrow metallic slit. *Phys. Rev. Lett.* **2002**, *89*, 063901.

(23) Hibbins, A. P.; Sambles, J. R.; Lawrence, C. R.; Brown, J. R. Squeezing millimeter waves into microns. *Phys. Rev. Lett.* **2004**, *92*, 143904.

(24) Lockyear, M. J.; Hibbins, A. P.; Sambles, J. R.; Lawrence, C. R. Microwave transmission through a single subwavelength annular aperture in a metal plate. *Phys. Rev. Lett.* **2005**, *94*, 193902.

(25) Aydin, K.; Cakmak, A. O.; Sahin, L.; Li, Z.; Bilotti, F.; Vegni, L.; Ozbay, E. Split-ring-resonator-coupled enhanced transmission through a single subwavelength aperture. *Phys. Rev. Lett.* **2009**, *102*, 013904.

(26) Moon, T.; Lee, B.; Kim, T.-G.; Oh, J.; Noh, Y. W.; Nam, S.; Park, B. Microwave dielectric relaxation of the polycrystalline (Ba,Sr)TiO_3 thin films. *Appl. Phys. Lett.* **2005**, *86*, 182904.

(27) Rosner, B. r. T.; van der Weide, D. W. High-frequency near-field microscopy. *Rev. Sci. Instrum.* **2002**, *73*, 2505−2525.

(28) Jenkins, M. D.; Naether, U.; Ciria, M.; Sesé, J.; Atkinson, J.; Sánchez-Azqueta, C.; Barco, E. d.; Majer, J.; Zueco, D.; Luis, F. Nanoscale constrictions in superconducting coplanar waveguide resonators. *Appl. Phys. Lett.* **2014**, *105*, 162601.

(29) Jeong, J.; Rhie, J.; Jeon, W.; Hwang, C. S.; Kim, D.-S. High-throughput fabrication of infinitely long 10 nm slit arrays for terahertz applications. *J. Infrared, Millimeter, Terahertz Waves* **2015**, *36*, 262−268.

DOI: 10.1021/acsphotonics.6b00047
ACS Photonics 2016, 3, 537−542

(30) Garcia-Vidal, F. J.; Moreno, E.; Porto, J. A.; Martin-Moreno, L. Transmission of light through a single rectangular hole. *Phys. Rev. Lett.* **2005**, *95*, 103901.
(31) Seo, M. A.; Park, H. R.; Koo, S. M.; Park, D. J.; Kang, J. H.; Suwal, O. K.; Choi, S. S.; Planken, P. C. M.; Park, G. S.; Park, N. K.; Park, Q. H.; Kim, D. S. Terahertz field enhancement by a metallic nano slit operating beyond the skin-depth limit. *Nat. Photonics* **2009**, *3*, 152−156.
(32) Kihm, H. W.; Koo, S. M.; Kim, Q. H.; Bao, K.; Kihm, J. E.; Bak, W. S.; Eah, S. H.; Lienau, C.; Kim, H.; Nordlander, P.; Halas, N. J.; Park, N. K.; Kim, D. S. Bethe-hole polarization analyser for the magnetic vector of light. *Nat. Commun.* **2011**, *2*, 451.
(33) Lee, D.; Kim, D. S. Light scattering of rectangular slot antennas: parallel magnetic vector vs perpendicular electric vector. *Sci. Rep.* **2016**, *6*, 18935.
(34) Seeger, K. Microwave dielectric constants of silicon, gallium arsenide, and quartz. *J. Appl. Phys.* **1988**, *63*, 5439−5443.
(35) Bolivar, P. H.; Brucherseifer, M.; Rivas, J. G.; Gonzalo, R.; Ederra, I.; Reynolds, A. L.; Holker, M.; de Maagt, P. Measurement of the dielectric constant and loss tangent of high dielectric-constant materials at terahertz frequencies. *IEEE Trans. Microwave Theory Tech.* **2003**, *51*, 1062−1066.
(36) Lin, J.; Oh, S. H.; Nguyen, H. M.; Reitich, F. Field enhancement and saturation of millimeter waves inside a metallic nanogap. *Opt. Express* **2014**, *22*, 14402−14410.
(37) Bahk, Y. M.; Park, H. R.; Ahn, K. J.; Kim, H. S.; Ahn, Y. H.; Kim, D. S.; Bravo-Abad, J.; Martin-Moreno, L.; Garcia-Vidal, F. J. Anomalous band formation in arrays of terahertz nanoresonators. *Phys. Rev. Lett.* **2011**, *106*, 013902.
(38) Kang, J. H.; Choe, J.-H.; Kim, D. S.; Park, Q. H. Substrate effect on aperture resonances in a thin metal film. *Opt. Express* **2009**, *17*, 15652−15658.
(39) Gordon, R.; Brolo, A. G. Increased cut-off wavelength for a subwavelength hole in a real metal. *Opt. Express* **2005**, *13*, 1933−1938.
(40) Born, M.; Wolf, E.; Bhatia, A. B.; Gabor, D.; Stokes, A. R.; Taylor, A. M.; Wayman, P. A.; Wilcock, W. L. *Principles of Optics: Electromagnetic Theory of Propagation, Interference and Diffraction of Light*; Cambridge University Press, 2000; pp 359−366.
(41) Choi, S. B.; Park, D. J.; Jeong, Y. K.; Yun, Y. C.; Jeong, M. S.; Byeon, C. C.; Kang, J. H.; Park, Q. H.; Kim, D. S. Directional control of surface plasmon polariton waves propagating through an asymmetric Bragg resonator. *Appl. Phys. Lett.* **2009**, *94*, 063115.
(42) Han, S.; Bahk, Y. M.; Park, N.; Kim, D. S. Terahertz field enhancement in asymmetric and tapered nano-gaps. *Opt. Express* **2016**, *24*, 2065−2071.
(43) Lee, J. W.; Seo, M. A.; Kang, D. H.; Khim, K. S.; Jeoung, S. C.; Kim, D. S. Terahertz electromagnetic wave transmission through random arrays of single rectangular holes and slits in thin metallic sheets. *Phys. Rev. Lett.* **2007**, *99*, 137401.
(44) Park, H.-R.; Bahk, Y.-M.; Ahn, K. J.; Park, Q. H.; Kim, D.-S.; Martín-Moreno, L.; García-Vidal, F. J.; Bravo-Abad, J. Controlling Terahertz Radiation with Nanoscale Metal Barriers Embedded in Nano Slot Antennas. *ACS Nano* **2011**, *5*, 8340−8345.
(45) Park, H. R.; Bahk, Y. M.; Choe, J. H.; Han, S.; Choi, S. S.; Ahn, K. J.; Park, N.; Park, Q. H.; Kim, D. S. Terahertz pinch harmonics enabled by single nano rods. *Opt. Express* **2011**, *19*, 24775−24781.

DOI: 10.1021/acsphotonics.6b00047
ACS Photonics 2016, 3, 537−542